

In-plane oriented $CH_3NH_3PbI_3$ nanowire suppression of the interface electron transfer to PCBM

Tao Wang(王涛), Zhao-Hui Yu(于朝辉), Hao Huang(黄昊), Wei-Guang Kong(孔伟光), Wei Dang(党伟), and Xiao-Hui Zhao(赵晓辉)

Citation: Chin. Phys. B, 2021, 30 (**6**): 066801. DOI: 10.1088/1674-1056/abf4fa
Journal homepage: http://cpb.iphy.ac.cn; http://iopscience.iop.org/cpb

What follows is a list of articles you may be interested in

Temperature-dependent subband mobility characteristics in n-doped silicon junctionless nanowire transistor

Ya-Mei Dou(窦亚梅), Wei-Hua Han(韩伟华), Yang-Yan Guo(郭仰岩), Xiao-Song Zhao(赵晓松), Xiao-Di Zhang(张晓迪), Xin-Yu Wu(吴歆宇), Fu-Hua Yang(杨富华)
Chin. Phys. B, 2019, 28 (**6**): 066804. DOI: 10.1088/1674-1056/28/6/066804

Full filling of mesoporous carbon nanotubes by aqueous solution at room temperature

Xiao-Na Ren(任晓娜), Min Xia(夏敏), Qing-Zhi Yan(燕青芝), Chang-Chun Ge(葛昌纯)
Chin. Phys. B, 2019, 28 (**3**): 036801. DOI: 10.1088/1674-1056/28/3/036801

Surface effects on the thermal conductivity of silicon nanowires

Hai-Peng Li(李海鹏), Rui-Qin Zhang(张瑞勤)
Chin. Phys. B, 2018, 27 (**3**): 036801. DOI: 10.1088/1674-1056/27/3/036801

An effective-field theory study of hexagonal Ising nanowire：Thermal and magnetic properties

Yusuf Kocakaplan, Ersin Kantar
Chin. Phys. B, 2014, 23 (**4**): 046801. DOI: 10.1088/1674-1056/23/4/046801

In-plane oriented $CH_3NH_3PbI_3$ nanowire suppression of the interface electron transfer to PCBM*

Tao Wang(王涛), Zhao-Hui Yu(于朝辉), Hao Huang(黄昊),
Wei-Guang Kong(孔伟光), Wei Dang(党伟)†, and Xiao-Hui Zhao(赵晓辉)‡

Hebei Key Laboratory of Optic-Electronic Information Materials, College of Physics Science and Technology, Hebei University, Baoding 071002, *China*

(Received 1 January 2021; revised manuscript received 22 March 2021; accepted manuscript online 6 April 2021)

One-dimensional nanowire is an important candidate for lead-halide perovskite-based photonic detectors and solar cells. Its surface population, diameter, and growth direction, *etc.*, are critical for device performance. In this research, we carried out a detailed study on electron transfer process at the interface of nanowire $CH_3NH_3PbI_3$(N-$MAPbI_3$)/Phenyl C61 butyric acid methyl-ester synonym (PCBM), as well as the interface of compact $CH_3NH_3PbI_3$(C-$MAPbI_3$)/PCBM by transient absorption spectroscopy. By comparing the carrier recombination dynamics of N-$MAPbI_3$, N-$MAPbI_3$/PCBM, C-$MAPbI_3$, and C-$MAPbI_3$/PCBM from picosecond (ps) to hundred nanosecond (ns) time scale, it is demonstrated that electron transfer at N-$MAPbI_3$/PCBM interface is less efficient than that at C-$MAPbI_3$/PCBM interface. In addition, electron transfer efficiency at C-$MAPbI_3$/PCBM interface was found to be excitation density-dependent, and it reduces with photo-generation carrier concentration increasing in a range from 1.0×10^{18} cm^{-3}–4.0×10^{18} cm^{-3}. Hot electron transfer, which leads to acceleration of electron transfer between the interfaces, was also visualized as carrier concentration increases from 1.0×10^{18} cm^{-3}–2.2×10^{18} cm^{-3}.

Keywords: lead-halide perovskite, nanowire, interface electron transfer, transient absorption spectroscopy

PACS: 68.35.bj, 68.55.ag, 72.20.Jv **DOI:** 10.1088/1674-1056/abf4fa

1. Introduction

Perovskite solar cells (PSCs) belong to a new generation of solar cells, whose champion power conversion efficiency (PCE) has reached to 25.2%.[1] The perovskite film has also shown excellent performance in the field of photoelectrical detector, light-emitting diode, and x-ray detector.[2–6] In these applications, improving the interface charge separation efficiency is of great importance.[7,8] So far, various strategies such as hot casting, solvent annealing, mixed solvents technique, anti-solvent dripping, and the interface engineering have been developed for optimizing the perovskite film morphology.[9–12] Compared to compact perovskite film (C-PVK), nanowire perovskite film (N-PVK) exhibits significant advantages, such as superior anti-reflection, significant light trapping, and enhanced carrier transport, which are all beneficial for applications in opto-electronics.[13,14] N-$MAPbI_3$ films were first employed by Forro *et al.* in the field of light-emitting transistors.[15] The first N-$MAPbI_3$-based solar cell shows a more efficient interface transfer efficiency than that of typical C-PVK film and provides a 14.17% PCE.[16] Later on, N-PVK was more used in photodetector for its better oriented carrier transport.[17–20] Only a few of investigations of N-PVK-based solar cells have been performed. One report by Kilwon Cho *et al.* claimed that the fine control of the morphology of N-$MAPbI_3$ (diameter, surface coverage, distribution at surface or bulk) is required for optimum N-$MAPbI_3$-based solar cells.[21] Another research pointed out that the N-$MAPbI_3$ film has a lower interface charge transfer efficiency than that of nanocube and nanowire hybrid film.[14] The above two references stressed that more gaps and holes in N-PVK lead to loose contact between N-PVK and the charge transport materials, which results in lower PCE. However, to the best of our knowledge, there are few relevant dynamic experiments for such a judgement. In consideration of widely use of N-PVK in solar cells and photodetectors, its interface charge transfer dynamics deserves a more detailed investigation.

In this paper, interface electron transfer dynamics from C-$MAPbI_3$ film, as well as in-plane oriented N-$MAPbI_3$ film to PCBM were studied by using femtosecond transient absorption spectroscopy. The target carrier recombination dynamics were extracted from probe wavelength where the induced refractive change can hardly affect the transmitted light intensity. An efficient interface charge transfer phenomenon between C-$MAPbI_3$ film and PCBM was demonstrated in ours experimental results. While efficient interface electron transfer was absent from N-$MAPbI_3$/PCBM interface, no matter of carrier generation density or observation time scales from

*Projected supported by the National Natural Science Foundation of China (Grant Nos. 21503066 and 61904048), the Fundamental Research Project from Shenzhen Science and Technology Innovation Committee (Grant No. JCYJ20180302174021198), the Natural Science Foundation of Hebei Province, China (Grant No. F2017201136), and the Foundation of Hebei Educational Committee (Grant No. ZC2016003).

†Corresponding author. E-mail: dangwei@hbu.edu.cn

‡Corresponding author. E-mail: xhzhao@hbu.edu.cn

© 2021 Chinese Physical Society and IOP Publishing Ltd

some picosecond to tens nanosecond. Hot electron transfer at C-$MAPbI_3$/PCBM interface was detected in excitation density varying experiment. The hot electron transfer accelerates the decay of carrier concentration of C-$MAPbI_3$ in first 10 ps–20 ps.

2. Experimental section

2.1. Materials

Methylammonium iodide (MAI, purity $>$ 99.99%) and lead (II) iodide (PbI_2, purity $>$ 99.99%) were bought from Xi'an Polymer Light Technology Corp. Isopropanol (IPA, purity $>$ 99.8%), toluene(AR), N,N-Dimethylformamide (DMF, purity $>$ 99.8%, Sigma), 1-Methyl-2-pyrrolidone (NMP, purity $>$ 99.5%, Sigma) Chlorobenzene (CB, purity $>$ 99.99%, Kermel) are all kept in a N_2-filled glovebox before use. The indium tin oxide (ITO) glasses were bought from South China Xiang Science & Technology Company Limited.

The ITO glass substrates were first cleaned with detergent, then were successively washed with deionized water, isopropanol, deionized water, acetone, and isopropanol in an ultrasonication bath at 30 °C for 20 min, and finally were dried with nitrogen flow. After treated with oxygen plasma (30 min), the substrates were transferred to a N_2-filled glovebox for further use.

2.2. Compact $MAPbI_3$ film

The 1-ml $MAPbI_3$ precursor solution was prepared by dissolving 580-mg PbI_2 and 200-mg MAI in the mixed solvent of 600-μL DMF and 400-μL NMP, and then was stirred overnight at 30 °C. 35 μL of $MAPbI_3$ solution was spin-coated on the substrate at 1000 rpm for 8 s and 4000 rpm for 12 s. At the 4th second before the end 75 μL of toluene solution was dipped to achieve a smooth surface. And the as-prepared $MAPbI_3$ film was kept alone for 30 min, then it was annealed at 90 °C for 9 min. The average thickness of C-$MAPbI_3$ is about 400 nm.

2.3. Nanowire $MAPbI_3$ film

The 1-ml PbI_2 solution was prepared by dissolving 462-mg PbI_2 in 1-mL DMF, and then it was stirred over night at 30 °C for use. The 1-ml MAI solution was prepared by dissolving 10-mg MAI in mixed solution of 1000-μL isopropanol and 50-μL DMF, and also it was stirred overnight at 30 °C for use. The 30 μL of PbI_2 solution of 70 °C was spin-coated on the prepared substrate at 3000 rpm for 5 s and 6000 rpm for 5 s. After kept alone for 10 min the as-prepared PbI_2 film was annealed at 70 °C for 3 min, then it was cooled down to room temperature. The 70 μL of MAI solution was loaded on the PbI_2 and kept alone for 4 s, then it was spun at 1500 rpm for 20 s and kept alone 15 min till the color of as-prepared film completely turned to dark-brown from light-brown, then annealed at 100 °C for 5 min. The average thickness of N-$MAPbI_3$ is about 300 nm.

2.4. PCBM treatment film

PCBM solution was prepared by dissolving 20 mg of PCBM in 1 mL of chlorobenzene. When the perovskite film was cooled down from annealing for 5 min, the as-prepared PCBM solutions were dripped onto the perovskite layer, then the film was spun at a speed of 1500 rpm for 30 s.

2.5. Characterizations

The ultraviolet-visible (UV-vis) absorption spectra were recorded by UV-2600 (Shimazu). Scanning electron microscope (SEM) images were obtained by Zeiss Sigma at a 3.0-kV accelerating voltage. The surface morphology was measured by atomic force microscopy (AFM, Multimode 8, Bruker). The thickness of the film was measured by a step profiler (Dektak-XT Bruker). The x-ray diffraction (XRD) patterns were measured by a D/max 2400 x-ray diffractometer with Cu Kα radiation (λ = 1.54050 Å). The photoluminescence (PL) measurement uses a CW laser (532 nm) as excitation source and the emission from perovskite film was recorded by a liquid nitrogen cooled CCD detector array attached to an Acton SP 2500 spectrometer. Time-resolved photoluminescence (TRPL) was recorded by a frequency-domain fluorometry with excitation wavelength at 405 nm.

2.6. Transient absorption spectrum measurement

Femtosecond transient absorption spectra measurements were conducted using a femtosecond laser (Spirtfire ACE 100F 800 nm, full width at half maximum (FWHM) pulse width 100 fs, 1-kHz repetition rate) and an ultrafast spectroscopic system (Harpia). The output of fundamental laser was split into pump (95%) and probe (5%) beams. The pump beam was directed through an optical parametric amplification system (TOPAS Prime-F) to generate 550-nm pump beam, while the probe beam was passed through an optical delay rail and focused onto a Ti:sapphire crystal to generate a white light continuum. The angle between polarization directions of pump beam and probe beam was set up as magic angle 54.7° and the optical delay stage provided a probe time window of 8 ns.

3. Results and discussion

The surface morphologies of both types of $MAPbI_3$ film are shown in Fig. 1. As shown in Fig. 1(a), the surface of N-$MAPbI_3$ is uniformly covered by nanowires. Its extended view in the inset shows that most of N-$MAPbI_3$ nanowires are in-plane-oriented and amount of gaps and holes exists between them. The C-$MAPbI_3$ is in poly-crystal form, which looks like $MAPbI_3$ riprap (Fig. 1(b)). The diameter of grain crystal is in

the order of hundreds of nanometers. According to AFM measurement, the roughness R_q of C-MAPbI$_3$ is 3.76 nm, much smaller than R_q 57.2 nm of N-MAPbI$_3$.

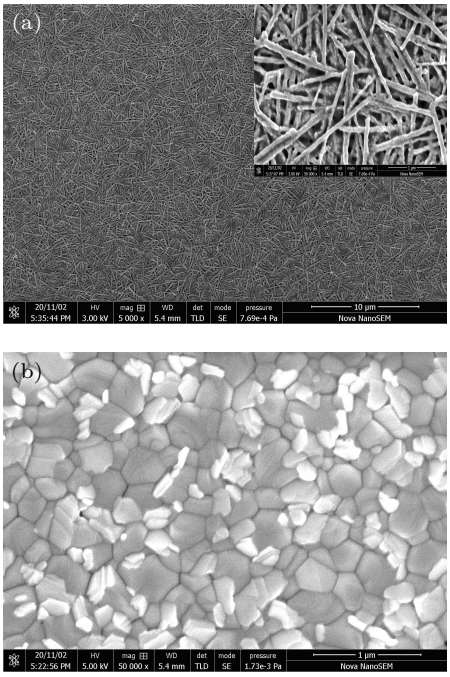


Fig. 1. SEM images of N-MAPbI$_3$ (a) and C-MAPbI$_3$ (b), the inset in panel (a) shows an extend view of N-MAPbI$_3$.

The XRD patterns of C-MAPbI$_3$ and N-MAPbI$_3$ are shown in Fig. 2. The patterns of both C-MAPbI$_3$ and N-MAPbI$_3$ contain diffraction plane (110) and (220) peaks at 14.2° and 28.7°, which indicate preferential tetragonal structure. Other noticeable differences in N-MAPbI$_3$ with respect to C-MAPbI$_3$ includes a weaker (220) peak and stronger (112), (211), (202), and (310) peaks, indicating different morphologies between them. It is should be noted that the XRD peak at 12.6° in N-MAPbI$_3$ originates from residual PbI$_2$, because the amount of MAI was limited in preparation of N-MAPbI$_3$ by two-step method. The residual PbI$_2$ mainly locates near the substrate and does not affect interface charge transfer from N-MAPbI$_3$ to PCBM.

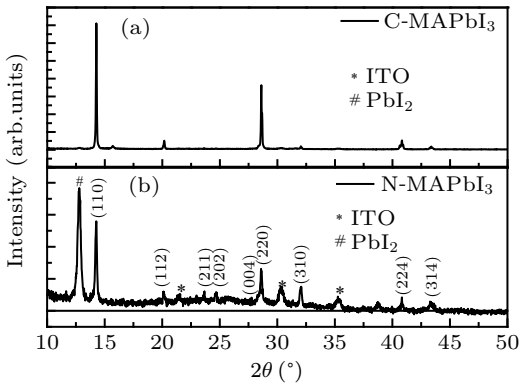


Fig. 2. XRD patterns of C-MAPbI$_3$ (a) and N-MAPbI$_3$ (b).

Steady absorption spectra of C-MAPbI$_3$, N-MAPbI$_3$, and their counterparts covered by PCBM are shown in Fig. 3. Both exciton absorptions of C-MAPbI$_3$ and N-MAPbI$_3$ films locate at about 750 nm.[22] A remarkable absorbance from 750 nm to 800 nm in N-MAPbI$_3$ film was attributed to surface scattering, not sub-bandgap absorption.[23] This attribution is in consistent with similar PL spectra of C-MAPbI$_3$ and N-MAPbI$_3$ (Fig. 3). The PCBM coating does not affect steady PL of C-MAPbI$_3$ film, but leads a little blue shift of PL of N-MAPbI$_3$ (Fig. S1). It is consistent with the reported passivation effect of PCBM on trap states in MAPbI$_3$.[24]

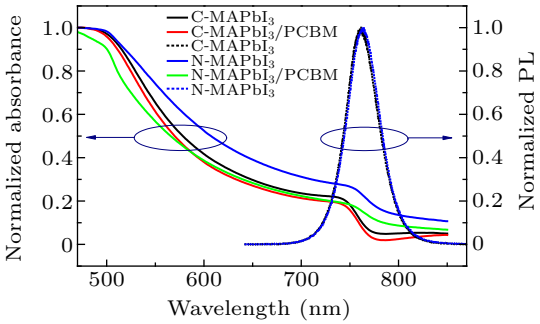


Fig. 3. Steady absorption spectra of C-MAPbI$_3$ (black solid line), C-MAPbI$_3$/PCBM (red solid line), N-MAPbI$_3$ (blue solid line), N-MAPbI$_3$/PCBM (green solid line), and steady PL of C-MAPbI$_3$ (black dash line), N-MAPbI$_3$ (blue dash line).

To observe charge recombination in MAPbI$_3$ and electron transfer to PCBM at its interface, transient absorption spectroscopy is a powerful tool. Typical transient absorption spectra at some time delays for C-MAPbI$_3$ and N-MAPbI$_3$ are presented in Figs. 4(a) and 4(c). Both transient absorption spectra of C-MAPbI$_3$ and N-MAPbI$_3$ show similar features, with a ground state bleach (GSB) signal centered at 760 nm and a broad photo-induced absorption (PIA) signal around 600 nm. Within the first 1 ps, isosbestic point of their transient absorption spectra appears blue shifts first, then red shifts successively due to hot carrier cooling.[25] Transient absorption spectra of C-MAPbI$_3$/PCBM and N-MAPbI$_3$/PCBM have also been presented in Fig. S2. They have similar spectral features with their counterparts without PCBM covering in our monitoring wavelength range.

We compared kinetics of absorbance change (ΔmOD) for C-MAPbI$_3$ film, N-MAPbI$_3$ film, and their counterparts with PCBM covering. Monitoring wavelengths were selected at 601 nm (PIA) and 761 nm (GSB). PCBM has a small absorbance at 550 nm (Fig. S3), and its transient absorption signals at 601 nm and 761 nm are much smaller with respect to that of MAPbI$_3$ (Fig. S4). Therefore, the absorbance changes (ΔmOD) of four types films at 601 nm and 761 nm are only related to the charge carrier concentration in MAPbI$_3$. The kinetic traces of C-MAPbI$_3$ and N-MAPbI$_3$ were compared in Fig. S5 in the Supplementary materials. N-MAPbI$_3$ film displays more faster decay in kinetics traces at the 601 nm (PIA) and 760 nm (GSB), indicating a shorter carrier lifetime than that of C-MAPbI$_3$ film. The comparison of kinetic traces of

C-MAPbI$_3$ and C-MAPbI$_3$/PCBM are presented in Fig. 4(b). Obviously, C-MAPbI$_3$/PCBM kinetics traces at 601 nm (PIA) and 760 nm (GSB) show much faster decays. This is the evidence of interface electron transfer from C-MAPbI$_3$ to PCBM, which reduces the carrier lifetime of MAPbI$_3$. But the faster decay of absorbance change (ΔmOD) of C-MAPbI$_3$/PCBM is only sustained for about 20 ps according to Fig. 4(b) and Fig. S6. It means electron transfer rate decreases with time. The mechanism of this fast electron transfer process would be explained later.

In contrast to C-MAPbI$_3$, the kinetics of absorbance change (ΔmOD) of N-MAPbI$_3$/PCBM was nearly overlaid with that of N-MAPbI$_3$ film at first 20-ps time scale (Fig. 4(d)) and nanosecond scale(Fig. S7). It seems that electron transfer at N-MAPbI$_3$/PCBM interface is less efficient than that of C-MAPbI$_3$/PCBM.

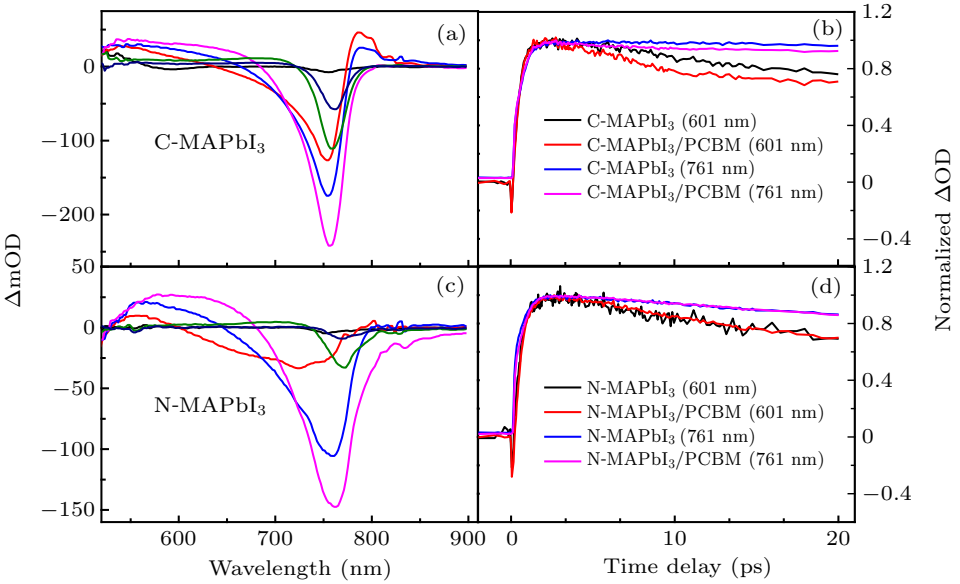


Fig. 4. Panels (a) and (c) are differential transmission spectra (mOD) for C-MAPbI$_3$ and N-MAPbI$_3$ films after excitation at 550 nm (1 kHz, 100 fs, 155 μJ/cm^2): black (0 ps), red (0.3 ps), blue (0.6 ps), magenta (1.24 ps), olive (919.95 ps), and navy (4049.95 ps). Panels (b) and (d) are normalized photo-induced absorption kinetics (601 nm) and negative bleaching kinetics (761 nm) of C-MAPbI$_3$ and N-MAPbI$_3$ films.

We also checked the electron transfer process at C-MAPbI$_3$/PCBM interface and N-MAPbI$_3$/PCBM interface at hundreds of nanoseconds time scales by use of TRPL technique, as shown in Fig. 5. All TRPL decay curves were fitted by multiple exponential decay function. Detailed fitting parameters are shown in Table S1. The PL lifetime of the C-MAPbI$_3$ film is 128.5 ns, and it decreases to 20.68 ns as being covered by PCBM. By contrast, the PL lifetime of N-MAPbI$_3$ is 10.62 ns that is very close to the PL lifetime (9.26 ns) for N-MAPbI$_3$/PCBM. TRPL measurements also confirm a less efficient electron transfer at N-MAPbI$_3$/PCBM interface than that of C-MAPbI$_3$/PCBM interface. At MAPbI$_3$/PCBM interface, carrier transfer process is coexisted and competes with carrier recombination in MAPbI$_3$. We attribute more efficient electron transfers at C-MAPbI$_3$/PCBM interface to close contact between C-MAPbI$_3$ and PCBM and longer carrier lifetime in C-MAPbI$_3$ (Fig. S5 and Fig. 5). While N-MAPbI$_3$ shows loose contact with PCBM and shorter carrier lifetime, both of which are disadvantages for the interface electron transfer. In addition, MAPbI$_3$ nano-wire inherits a better diffusion coefficient than that of MAPbI$_3$ film.[26] Thus carriers in in-plane-oriented N-MAPbI$_3$ diffuse along radial direction more faster than that of C-MAPbI$_3$, lowering the carrier concentration at the interface. We suppose it as another disadvantage for N-MAPbI$_3$ nanowire investigated in this research.

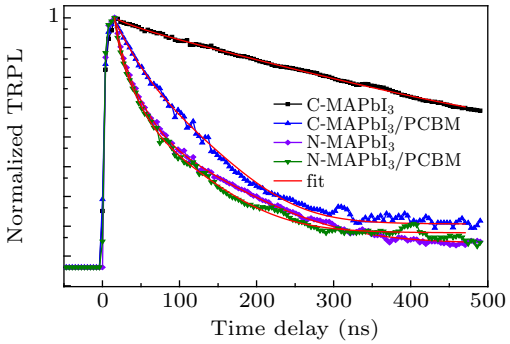


Fig. 5. TRPL decay curves of C-MAPbI$_3$ (black line and square), C-MAPbI$_3$/PCBM (blue line and triangle), N-MAPbI$_3$ (purple line and diamond), and N-MAPbI$_3$/PCBM (green line and triangle) and their fitting (red line).

The interface charge transfer between MAPbI$_3$ and electron transfer material or hole transfer material undergoes a competition with charge trapping and recombination within MAPbI$_3$. It has been reported that interface charge transfer efficiency is highly dependent on the excitation density.[27,28] In lighting this, here we also checked the effect of carrier concentration on the charge transfer between C-MAPbI$_3$ and PCBM. Kinetics at 601 nm (PIA) was chosen for such analyzation for its shorter rising phase in time than that of 761 nm (GSB) (Fig. S5) and less interference with transient reflectivity than

that of 761nm (GSB) (Fig. S8).

All kinetics at 601 nm (PIA) of C-MAPbI$_3$ and C-MAPbI$_3$/PCBM under three different excitation densities were fitted with the convolution of Gaussian function and three exponential decays function, as shown Figs. 6(a)–6(c). Fitting parameters of three time components are shown in Table 1 and their standard errors are supplied in Table S1. Three features can be observed from fitting results in Table 2. Firstly, the addition of PCBM induces a reduction in all time constants when a low excitation density of 70 μJ/cm^2 is used. Secondly, at medium excitation density of 155 μJ/cm^2, the addition of PCBM only induces a reduction in the fastest time component (10 ps–20 ps). Thirdly, the addition of PCBM does not change the time constants obviously as the excitation density is as high as 284 μJ/cm^2. According to reduction of average carrier lifetime of C-MAPbI$_3$ in Table 1, higher electron transfer efficiency to PCBM occurs with low and medium excitation density.

In our transient absorption measurement (see Figs. 6(a)–6(c)), the photo-generate carrier density is estimated as 1.0×10^{18} cm^{-3}, 2.2×10^{18} cm^{-3}, and 4.0×10^{18} cm^{-3}, respectively (using reflectivity $R = 0.17$, absorbance coefficient $\alpha = 10^5$ cm^{-1}, pump beam focus diameter 300 μm). It has been reported that Auger recombination becomes dominant at very high carrier density ($\geq 2 \times 10^{18}$ cm^{-3}–5×10^{18} cm^{-3}),[29,30] which is consistent with our experimental results in Fig. S9, The electron transfer from C-MAPbI$_3$ to PCBM we measured competes with Auger recombination and bi-molecule recombination. Higher carrier density accelerates carrier high order recombination within the MAPbI$_3$, leading the decrease of electron transfer efficiency.

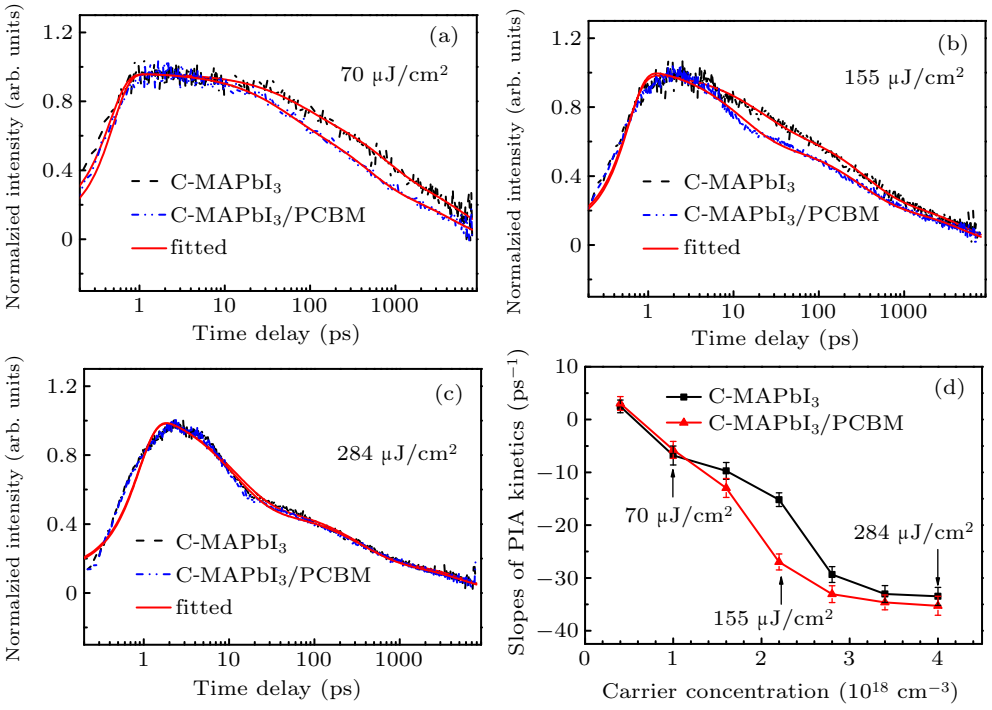


Fig. 6. Comparisons of photo-induced absorption kinetics (601 nm) for C-MAPbI$_3$ and C-MAPbI$_3$/PCBM under three excitation densities and their fittings [(a)–(c)], and dependence of slopes of kinetics (601 nm) for C-MAPbI$_3$ and C-MAPbI$_3$/PCBM in the first 10 ps–20 ps.

Table 1. Time components for C-MAPbI$_3$ and C-MAPbI$_3$/PCBM following multiple exponential decay fitting. Note that the carrier density affects the rising phase of kinetics of PIA at 601 nm, so different full width and half magnitudes (FWHM) of Gaussian function were used.

Excitation density (μJ/cm^2)	τ_1 (ps)	A_1	τ_2 (ps)	A_2	τ_3 (ps)	A_3	τ_{ava} (ps)	FWHM (ps)
	C-MAPbI$_3$							
70	67.3	0.205	638.4	0.363	6607.7	0.393	2957.7	0.25
155	19.0	0.306	319.2	0.416	5193.9	0.277	1578.9	0.3
284	11.6	0.538	309.0	0.309	6320.0	0.198	1294.8	0.5
	C-MAPbI$_3$/PCBM							
70	44.2	0.259	405.4	0.392	4594.1	0.313	1668.0	0.25
155	11.8	0.428	293.6	0.363	4930.4	0.238	1248.85	0.3
284	11.2	0.574	342.0	0.291	5904.5	0.188	1154.0	0.5

The electron transfer time can be estimated as the difference of the reciprocal of carrier density decay lifetime with and without PCBM covering,[31] as shown in the formula

$$\frac{1}{\tau_{\text{transfer}}} = \frac{1}{\tau_{\text{pve/PCBM}}} - \frac{1}{\tau_{\text{pev}}}, \tag{1}$$

where τ_{pev} is the decay lifetime of the carrier in C-MAPbI$_3$, $\tau_{\text{pve/PCBM}}$ is the decay lifetime of the carrier in C-MAPbI$_3$/PCBM, τ_{transfer} is the electron transfer lifetime. Under the excitation density of 70 μJ/cm^2, carrier concentration decay in C-MAPbI$_3$ was fitted well by use of three components with decay lifetime of 67.3 ps (44.2 ps), 683.4 ps (405.4 ps), and 6607.7 ps (4594.1 ps), respectively. These decay lifetimes indicate decay rates of carrier concentration at different time delays after photo excitation, and were determined by the residual carrier concentration in C-MAPbI$_3$. According to these decay lifetimes and formula (1), the electron transfer lifetimes between C-MAPbI$_3$ and PCBM interface were estimated as 128.8 ps, 997.0 ps, and 1.5×10^4 ps, which respectively corresponds to the three stages of carrier recombination process. Obviously, the electron transfer lifetime between C-MAPbI$_3$ and PCBM increases with carrier concentration decrease. As the carrier concentration decreases to the level that used in our TRPL measurement, the electron transfer time increases to 24.6×10^4 ps.

Finally we focus on the faster electron transfer between C-MAPbI$_3$/PCBM interface under excitation density of 155 μJ/cm^2 (see Figs. 4(b) and 6), where carrier concentration decay lifetime of C-MAPbI$_3$ reduces from 19.0 ps to 11.8 ps (see Table 1) with covering by PCBM. Correspondingly, carrier concentration decay lifetime of C-MAPbI$_3$ under excitation density of 70 μJ/cm^2 reduces from 67.3 ps to 44.2 ps (see Table 1). By use of formula (1), the electron transfer lifetime τ_{transfer} between C-MAPbI$_3$ and PCBM in the first tens picosecond time scale is 31.8 ps under excitation density of 155 μJ/cm^2. It is only the one fourth of electron transfer lifetime under excitation density of 70 μJ/cm^2, 128.8 ps. The contrast between electron transfer lifetime under two excitation densities demonstrates that much faster electron transfer rate occurs as higher excitation density (155 μJ/cm^2), though the total electron transfer efficiency is higher in lower excitation density condition (70 μJ/cm^2).

We have confirmed that higher carrier concentration can enhance interface electron transfer rate between C-MAPbI$_3$/PCBM. Yet this mechanism cannot be fully explained the faster electron transfer process under excitation density of 155 μJ/cm^2, because no sensible electron transfer process can be observed in hundreds picosecond time scale and hundred nanosecond time scale under this excitation density (see Table 1, τ_2, τ_3 for C-MAPbI$_3$ and C-MAPbI$_3$/PCBM). If the faster electron transfer process actually induced by higher carrier concentration, the sensible electron transfer process should also occur at C-MAPbI$_3$/PCBM interface in hundreds picosecond time scale and hundred nanosecond time scale. In addition, in the disordered MAPbI$_3$ film the carrier mobility increases with excitation density due to trap state filling.[32,33] But carrier densities in C-MAPbI$_3$ under 70 μJ/cm^2 and 155 μJ/cm^2 are both larger than trapped state population ($\sim 10^{14}$ cm^{-3}–10^{17} cm^{-3}),[34,35] and difference between carrier mobilities under both excitation density should not be enough to lead the faster electron transfer process in condition of excitation density 155 μJ/cm^2. We calculated slopes of kinetics (PIA) at 601 nm for C-MAPbI$_3$ and C-MAPbI$_3$/PCBM in the first 10 ps–20 ps time scale (Fig. S9), as shown in Fig. 6(d). Here we use the slope of kinetics to qualitatively character the decay rate of carrier concentration in C-MAPbI$_3$. We found that difference of slopes of kinetics enlarges with carrier concentration increasing in range of 4×10^{17} cm^{-3} to 2.2×10^{18} cm^{-3}, indicating acceleration of electron transfer with carrier concentration increase. What is more, rising phases of kinetics (PIA) at 601 nm also extend at higher carrier concentration (Fig. S9), which implies increase of carrier cooling time.[36,37] Hot carrier was viewed as beneficial to charge transfer to electron or hole transfer process.[38–40] In our measurement, energy of pump photons is about 0.65 eV above the band gap of MAPbI$_3$. Therefore, we cautiously proposed that faster electron transfer from C-MAPbI$_3$ to PCBM observed as carrier concentration in a range from 1.6×10^{18} cm^{-3} to 2.8×10^{18} cm^{-3} originates from hot electron transfer between the interfaces.

4. Conclusion

We have studied the electron transfer processes at the interface of C-MAPbI$_3$/PCBM and N-MAPbI$_3$/PCBM by use of femtosecond transient absorption spectroscopy and TRPL technique. An efficient electron transfer was observed at the C-MAPbI$_3$/PCBM interface. While at N-MAPbI$_3$/PCBM interface, no efficient electron transfer process can be detected from some picosecond time scale to hundred ns time scale. We prone to view the shorter carrier lifetime in N-MAPbI$_3$, loose contact between N-MAPbI$_3$ and PCBM at interface and excellent carrier transport in the plane direction as the leading causes for less efficient electron transfer at N-MAPbI$_3$/PCBM interface. We also investigated the influence of carrier concentration on interface electron transfer between C-MAPbI$_3$/PCBM. The interface electron transfer efficient drops with carrier concentration increase from 1.0×10^{18} cm^{-3} to 4.0×10^{18} cm^{-3} due to acceleration of carrier high order recombination within the C-MAPbI$_3$. Hot electron transfer was revealed by excitation density varying transient absorption spectrum measurement. Application of N-MAPbI$_3$ in solar cell or photoelectrical detector deserves

a fine interface morphology control, including a close contact between N-$MAPbI_3$ and charge transport layer, vertical growth of N-$MAPbI_3$ to the interface, decrease defect concentration to extend carrier lifetime, and explore use of hot carrier transfer at the interface.

References

[1] Chart of Best Research-Cell Efficiencies Provided by NREL http://www.nrel.gov/pv/assets/images/efficiency_chart.jpg

[2] Zhao J J, Zhao L, Deng Y H, Xiao X, Ni Z Y, Xu S and Huang J S 2020 *Nat. Photon.* **14** 612

[3] Zhang C X, Wang S, Li X M, Yuan M J, Turyanska L and Yang X Y 2020 *Adv. Funct. Mater.* **30** 1910582

[4] Li C L, Wang H L, Wang F, Li T F, Xu M J, Wang H, Wang Z, Zhan X W, Hu W D and Shen L 2020 *Light Sci. Appl.* **9** 18508

[5] Li C L, Ma Y, Xiao Y F, Shen L and Ding L M 2020 *InfoMat.* **2** 1247

[6] Ye F, Lin H, Wu H D, Zhu L, Huang Z F, Ouyang D, Niu G D and Choy W C H 2018 *Adv. Funct. Mater.* **29** 1806984

[7] Shao S Y and Loi M A 2019 *Adv. Mater. Interfaces* **7** 1901469

[8] Wolff C M, Caprioglio P, Stolterfoht M and Neher D 2019 *Adv. Mater.* **31** 1902762

[9] Miyata A, Mitioglu A, Plochocka P, Portugall O, Wang J T W, Stranks S D, Snaith H J and Nicholas R J 2015 *Nat. Phys.* **11** 582

[10] Nie W, Tsai H, Asadpour R, Blancon J C, Neukirch A J, Gupta G, Crochet J J, Chhowalla M, Tretiak S, Alam M A, Wang H L and Mohite A D 2015 *Science* **347** 522

[11] Singh R, Suranagi S R, Kumar M and Shukla V K 2017 *J. Appl. Phys.* **122** 235302

[12] Bi C, Wang Q, Shao Y C, Yuan Y B, Xiao Z G and Huang J S 2015 *Nat. Commun.* **6** 7747

[13] Pan H, Chen P R, Shi B, Li Y C, Gao Q Y, Zhang L, Zhao Y, Huang Q and Zhang X D 2020 *Acta Phys. Sin.* **69** 077101 (in CHinese)

[14] Yin J, Sun Y B, Fu W L, Wang Y Q, Xi J T and Sun Y M 2016 *Mater. Lett.* **184** 78

[15] Horváth E, Spina M, Szekrényes Z, Kamarás K, Gaal R, Gachet D and Forró L 2014 *Nano Lett.* **14** 6761

[16] Im J H, Luo J S, Franckevicius M, Pellet N, Gao P, Moehl T, Zakeeruddin S M, Nazeeruddin M K, Gratzel M and Park N G 2015 *Nano Lett.* **15** 2120

[17] Zhu P C, Gu S, Shen X P, Xu N, Tan Y L, Zhuang S D, Deng Y, Lu Z D, Wang Z L and Zhu J 2016 *Nano Lett.* **16** 871

[18] Deng W, Huang L M, Xu X Z, Zhang X J, Jin X C, Lee S T and Jie J S 2017 *Nano Lett.* **17** 2482

[19] Asuo, I M, Fourmont P, Ka I, Gedamu D, Bouzidi S, Pignolet A, Riad R and Cloutier S G 2018 *Small* **15** 1804150

[20] Hu Q, Wu H, Sun J, Yan D H, Gao Y L and Yang J L 2016 *Nanoscale* **8** 5350

[21] Singh R B, Suranagi S R, Yang S J and Cho K 2018 *Nano Energy* **51** 192

[22] Saba M, Cadelano M, Marongiu D, Chen F P, Sarritzu V, Sestu N, Figus C, Aresti M, Piras R, Lehmann A G, Cannas C, Musinu A, Quochi F, Mura A and Bongiovanni G 2014 *Nat.Commun.* **5** 5049

[23] Tian Y X and Scheblykin I G 2015 *J. Phys. Chem. Lett.* **6** 3466

[24] Shao Y C, Xiao Z G, Bi C, Yuan Y B and Huang J S 2014 *Nat. Commun.* **5** 5784

[25] Madjet M E, Berdiyorov G R, El-Mellouhi F, Alharbi F H, Akimov A V and Kais S 2017 *J. Phys. Chem. Lett.* **8** 4439

[26] Tian W M, Zhao C Y, Leng J, Cui R R and Jin S Y 2015 *J. Am. Chem. Soc.* **137** 12458

[27] Makuta S, Liu M N, Endo M, Nishimura H, Wakamiyab A and Tachibana Y 2013 *J. Name.* **00** 1

[28] Kim J, Godin R, Dimitrov S D, Du T, Bryant D, McLachlan M A and Durrant J R 2018 *Adv. Energy Mater.* **8** 1802474

[29] Sum T C and Mathews N 2014 *Energy Environ. Sci.* **7** 2518

[30] Cadelano, Sarritzu V, Sestu N, Marongiu D, Chen F, Piras R, Corpino R, Carbonaro C M, Quochi F, Saba M, Mura A and Bongiovanni G 2015 *Adv. Opt. Mater.* **3** 1557

[31] Liu M, Endo M, Shimazaki A, Wakamiya A and Tachibana Y 2018 *J. Photopolym. Sci. Technol.* **31** 633

[32] Ščajev P, Miasojedovas S and Juršėnas S 2020 *J. Mater. Chem. C* **8** 10290

[33] Scajev P, Aleksiejunas R, Miasojedovas S, Nargelas S, Inoue M, Qin C J, Matsushima T, Adachi C and Jursenas S 2017 *J. Phys. Chem. C* **121** 21600

[34] Herz L M 2016 *Ann. Rev. Phys. Chem.* **67** 65

[35] Manser J S, Christians J A and Kamat P V 2016 *Chem. Rev.* **116** 12956

[36] Fu J H, Xu Q, Han G F, Wu B, Huan C H A, Leek M L and Sum T C 2017 *Nat. Commun.* **8** 1300

[37] Chauhan K K, Prodhan S, Ghosh D, Waghale P, Bhattacharyya S, Dutta P K and Datta P K 2020 *IEEE J. Photovolt* **10** 803

[38] Zhou M, Sarmiento J S, Fei C B and Wang H 2019 *J. Phys. Chem. C* **123** 22095

[39] Jiménez-López J, Puscher B M D, Guldi D M and Palomares E 2020 *J. Am. Chem. Soc.* **142** 1236

[40] Dursun I, Maity P, Yin J, Turedi B, Zhumekenov A A, Lee K J, Mohammed O F and Bakr O M 2019 *Adv. Energy Mater.* **9** 1900084